Journal of Marine Research, 57, 503–535, 1999

The lattice Boltzmann method as a basis for ocean circulation modeling

by Rick Salmon[1]

ABSTRACT

We construct a lattice Boltzmann model of a single-layer, "reduced gravity" ocean in a square basin, with shallow water or planetary geostrophic dynamics, and boundary conditions of no slip or no stress. When the volume of the moving upper layer is sufficiently small, the motionless lower layer outcrops over a broad area of the northern wind gyre, and the pattern of separated and isolated western boundary currents agrees with the theory of Veronis (1973). Because planetary geostrophic dynamics omit inertia, lattice Boltzmann solutions of the planetary geostrophic equations do not require a lattice with the high degree of symmetry needed to correctly represent the Reynolds stress. This property gives planetary geostrophic dynamics a significant computational advantage over the primitive equations, especially in three dimensions.

1. Introduction

Numerical ocean circulation modelers usually follow one of two strategies. Numerical models based upon the primitive equations represent the first strategy. In primitive equation models, inertia-gravity waves are present even though these waves are unimportant contributors to the large-scale ocean circulation. The presence of inertia-gravity waves severely limits the size of the time step in primitive equation models. However, because of the inertia-gravity waves, the primitive equations comprise relatively few diagnostic equations and are, therefore, relatively easy to code and solve.

The second strategy employs balanced dynamical equations like the quasi-geostrophic or semi-geostrophic equations. In numerical models based upon balanced dynamics, inertia-gravity waves are absent; therefore, the time step can be much larger. However, the approximations used to filter out the inertia-gravity waves require the solution of additional, typically elliptic, and frequently nonlinear diagnostic equations. The infinite propagation speed associated with the diagnostic equations is a direct result of the balance condition that filters out inertia-gravity waves. In complex geometry, that is, with realistic ocean bathymetry, the only practical methods for solving the diagnostic equations are iterative. Unfortunately, iterative solution of the diagnostic equations can be more difficult

1. Scripps Institution of Oceanography, University of California, La Jolla, California, 92093-0225, U.S.A. ***email: rsalmon@ucsd.edu***

and less efficient than time-stepping the primitive equations, even when the solutions themselves are nearly geostrophic.

Lattice Boltzmann methods (hereafter LB) offer a third modeling strategy that, unlike both the primitive and balanced dynamical equations, is completely prognostic. Thus LB ocean models contain not only inertia-gravity waves but sound waves as well. In fact, because LB models contain an arbitrary number of dependent variables (corresponding to the arbitrary number of links between neighboring lattice points), LB models typically contain more types of waves than are actually present in the dynamical equations of interest. These extra modes, which we shall call *fast modes,* play a role that is closely analogous to the role played by inertia-gravity waves in solutions of the primitive equations. Although unimportant contributors to the whole solution, the fast modes carry information rapidly throughout the flow, removing the need for diagnostic equations of any kind.

Despite the presence of many fast modes, LB methods are efficient because the fast modes can be made to propagate at speeds which, although much faster than the slow modes of real physical interest, are very much slower than, for example, the speed of real sound waves. Thus LB methods resemble still another well-known scheme for modeling balanced dynamics, in which fast modes are not removed but instead simply slowed down by making parameter adjustments to the physics. However, compared to other methods for slowing down fast waves, LB methods, which amount to a technique of slowing and *attenuation,* seem more sophisticated.

Usually, but perhaps mainly for historical reasons, we regard the LB equations as equations governing the average behavior of an underlying lattice gas. Lattice gases are highly idealized models of the complete molecular dynamics of real fluids. However, because much of the energy in lattice gases is thermal energy, lattice gases constitute rather noisy models of macroscopic fluids. A principal advantage of the LB method over the lattice gas method is that LB filters out this noise. Thus LB models are, in a sense, balanced models, which despite their many degrees of freedom and high proportion of fast modes, filter out the *ultra* fast modes corresponding to thermal motions.

The great practical advantage of LB models lies in the extraordinary simplicity of the LB equations, their numerical stability, and in the fact that the LB equations are *massively parallel:* At each timestep, the LB solution algorithm proceeds without consulting the conditions at the neighboring lattice points. Thus each lattice point could have its own processor. These practical advantages more than compensate for the extra storage associated with the greater number of dependent variables.

While it is their potential for parallel processing that virtually guarantees that LB methods will play an important role in ocean circulation modeling, it is their mathematical simplicity that seems most appealing. With only slight exaggeration, one could say that the LB method never requires the computation of a derivative. Nevertheless, one can *interpret* the LB equations as finite-difference approximations to a simple and completely hyper-

bolic system of quasi-linear equations. This hyperbolic system neatly expresses the two fundamental components of LB dynamics: the *propagation* (usually called *streaming*) of information between neighboring lattice points, and the rapid *relaxation* of the variables at each lattice point toward a state of local equilibrium. The specification of this equilibrium state corresponds to a prescription of the basic dynamics.

Despite these important practical advantages, the LB method remains somewhat inflexible, and this appears to be its primary disadvantage. For example, LB models almost inevitably contain a close approximation to the standard Navier-Stokes viscosity; there is as yet no LB method for replacing this standard viscosity with a "higher order eddy viscosity" of the type that has proved convenient in "large eddy simulations." (However, considering the problematic nature of higher order viscosities, particularly in the presence of boundaries, this may not be such a serious disadvantage.) More generally, despite the promising work of Ancona (1994) and others, there is as yet no cookbook method for applying LB methods to arbitrary systems of partial differential equations. However, it seems likely that greater use of LB methods for a greater variety of applications will gradually lead to further generalizations in the theory and subsequent improvements in the method.

In this paper, we apply the LB method to a simple model of ocean circulation—the so-called reduced gravity model for a homogeneous, wind-driven layer of fluid overlying a denser layer that remains at rest even where it lies exposed to the wind. This model has frequently been studied by oceanographers. Here, however, we regard it mainly as a tool to assess the value of LB methods as the basis for more complicated, three-dimensional ocean circulation models.

Section 2 offers a brief but self-contained introduction to LB theory using language that should appeal to oceanographers. For a more complete introduction to the theory, the reader should consult the excellent reviews by Benzi *et al.* (1992) and Chen and Doolen (1998), and the wonderful book by Rothman and Zaleski (1997).

In Section 3 we derive an 8-velocity LB model corresponding to the rotating shallow water equations. If terms corresponding to momentum advection are dropped from the LB formulae for the equilibrium populations of the particles, then the same model yields solutions of the planetary geostrophic equations.

Section 4 presents numerical solutions of the LB model for shallow water and planetary geostrophic dynamics in a square ocean basin with a two-gyre wind stress and boundary conditions of no slip or no stress. When the total volume of the moving fluid layer is sufficiently large, the moving layer covers the whole basin, as seen in Figure 3. However, when the upper layer volume is smaller (Figure 4), the lower layer outcrops over a broad region of the northern gyre, and both separated and isolated western boundary currents are present, in agreement with the theory of Veronis (1973).

In Section 5, we examine the solutions of a 4-velocity LB model of the planetary geostrophic equations, which requires half as much computation and storage as the

8-velocity model of Sections 3 and 4. In Sections 5 and 6, we speculate that the three-dimensional analogue of the 4-velocity model holds great promise as the basis for a three-dimensional global ocean circulation model.

Lattice gas models and LB models have been widely used in fluid mechanics for about ten years, and several applications treat problems of geophysical fluid dynamics. For example, Benzi *et al.* (1998) present results from a 512-processor LB calculation of Rayleigh-Benard convection on a 256^3 lattice. However, I have not seen the LB method applied to rotating flow. Since, therefore, few oceanographers are likely to be familiar with the LB method, this paper is designed to be as self-contained as possible.

2. The lattice Boltzmann method

We illustrate the lattice Boltzmann method by application to the uni-directional wave equation,

$$\frac{\partial h}{\partial t} + c_R(h)\frac{\partial h}{\partial x} = 0, \tag{2.1}$$

for $h(x, t)$ on the infinite domain $-\infty < x < +\infty$. Here, $c_R(h)$, a prescribed function, is the speed of the "real" waves. Of course, solutions of (2.1) generally become multivalued after a finite time unless a diffusion term is added to (2.1). Nevertheless, we begin by considering (2.1). Although this example is extremely simple, it illustrates nearly all of the important ideas needed for the more complicated cases of interest.

In the LB method we introduce two new dependent variables, $h_1(x, t)$ and $h_2(x, t)$, which are related to $h(x, t)$ by

$$h = h_1 + h_2. \tag{2.2}$$

The new dependent variables obey equations of the form

$$\begin{aligned} h_1(x + c\Delta t, t + \Delta t) &= h_1(x, t) - \lambda\Delta t(h_1(x, t) - h_1^{eq}(h)) \\ h_2(x - c\Delta t, t + \Delta t) &= h_2(x, t) - \lambda\Delta t(h_2(x, t) - h_2^{eq}(h)) \end{aligned} \tag{2.3}$$

where the constants c, Δt, and λ, and the functions $h_1^{eq}(h)$ and $h_2^{eq}(h)$ remain to be specified. The strategy is to define these functions and parameters such that solutions of (2.3) approximate the solutions of (2.1).

We can regard (2.3) as finite-difference equations for h_1 and h_2, defined at lattice points separated by

$$\Delta x = c\Delta t. \tag{2.4}$$

The h^{eq} terms couple (2.3) together. However, it is better to regard the discrete dynamics (2.3) as a cycle with two steps. The first step corresponds to the *collision*

$$\begin{aligned} h_1' &= h_1(x, t) - \lambda\Delta t(h_1(x, t) - h_1^{eq}(h)) \\ h_2' &= h_2(x, t) - \lambda\Delta t(h_2(x, t) - h_2^{eq}(h)) \end{aligned} \tag{2.5}$$

at each lattice point. The collision step relaxes each h_i toward its local equilibrium value $h_i^{eq}(h_1 + h_2)$, which remains to be defined. The primes denote the values immediately after the collision. The second step is a *streaming*

$$\begin{aligned} h_1(x + c\Delta t, t + \Delta t) &= h_1'(x, t) \\ h_2(x - c\Delta t, t + \Delta t) &= h_2'(x, t) \end{aligned} \tag{2.6}$$

to the neighboring lattice points. In the limit $\lambda \to 0$ of no collisions, h_1 propagates unchanged to the right at speed c, from one lattice point to the next in a time step, whereas h_2 propagates to the left at the same speed. This suggests that we regard h_1 as the population of rightward-moving particles, h_2 as the population of leftward-moving particles, and $h = h_1 + h_2$ as the total population.

As a first step, we investigate (2.3) in the usual manner of assessing finite-difference equations: We regard c as a fixed constant and consider the limit $\Delta t \to 0$, which then corresponds to the limit of small time step *and* small lattice spacing. For $\Delta t \to 0$, (2.3) take the form

$$\begin{aligned} \left(\frac{\partial}{\partial t} + c\frac{\partial}{\partial x}\right)h_1 &= -\lambda(h_1 - h_1^{eq}(h)) \\ \left(\frac{\partial}{\partial t} - c\frac{\partial}{\partial x}\right)h_2 &= -\lambda(h_2 - h_2^{eq}(h)) \end{aligned} \tag{2.7}$$

of characteristic equations; the characteristics are the lines of constant $x \pm ct$. In the limit $\lambda \to 0$ of no collisions, h_1 and h_2 are Riemann invariants. However, we shall see that the collision terms are actually very important. In the physically relevant regime of relatively large λ, the collision terms hold the populations h_i very close to their corresponding equilibrium values h_i^{eq}.

We manipulate (2.7) into a single equation for h, and then choose $h_1^{eq}(h)$ and $h_2^{eq}(h)$ so that this equation approximates the equation (2.1) of interest. Let

$$q \equiv h_1 - h_2, \tag{2.8}$$

and rewrite (2.7) in terms of h and q. By summing and differencing (2.7) we obtain

$$\frac{\partial h}{\partial t} + c\frac{\partial q}{\partial x} = -\lambda(h - h^{eq}(h)) \tag{2.9}$$

and

$$\frac{\partial q}{\partial t} + c\,\frac{\partial h}{\partial x} = -\lambda(q - q^{eq}(h)) \tag{2.10}$$

where

$$h^{eq} \equiv h_1^{eq} + h_2^{eq} \tag{2.11}$$

and

$$q^{eq} \equiv h_1^{eq} - h_2^{eq}. \tag{2.12}$$

We assume that the local equilibrium has the same h as the actual, slightly disequilibrium, state. That is,

$$h_1^{eq} + h_2^{eq} = h_1 + h_2 \equiv h. \tag{2.13}$$

Eq. (2.13) is the first of two equations that will determine the h_i^{eq}. Because of (2.13), the collisions (2.5) conserve the total population, and (2.9) becomes

$$\frac{\partial h}{\partial t} + c\,\frac{\partial q}{\partial x} = 0. \tag{2.14}$$

Thus, collision terms occur in the evolution equation (2.10) for q, but not in the equation (2.14) for h. This makes h the *slow mode* and q the *fast mode*.

To obtain a closed equation for h, we apply $\partial/\partial t + \lambda$ to (2.14) and use (2.10) to eliminate q. The result

$$h_{tt} - c^2 h_{xx} + \lambda\left(h_t + \frac{\partial}{\partial x}(cq^{eq}(h))\right) = 0. \tag{2.15}$$

We choose

$$q^{eq}(h) = \frac{1}{c}\int c_R(h)\,dh, \tag{2.16}$$

so that (2.15) becomes

$$h_{tt} - c^2 h_{xx} + \lambda(h_t + c_R(h)h_x) = 0. \tag{2.17}$$

Eq. (2.16) is the second of two equations that determine the h_i^{eq}. By (2.13) and (2.16),

$$\begin{aligned} h_1^{eq} &= \frac{h}{2} + \frac{1}{2c}\int c_R(h)\,dh \\ h_2^{eq} &= \frac{h}{2} - \frac{1}{2c}\int c_R(h)\,dh. \end{aligned} \tag{2.18}$$

If we take the lattice spacing Δx as given, then, by (2.4), the choice of c corresponds to the choice of time step Δt. Thus the LB dynamics (2.3) is completely specified by (2.18) and the choice of c and λ.

Eq. (2.17) represents the sum of the "textbook" wave equation, with propagation speed c, plus λ multiplied by the equation (2.1) of interest. Therefore we should choose λ large enough so that the last two terms in (2.17) dominate the first two terms. The second term in (2.17) is a diffusion term of the kind required to keep (2.1) well behaved. On the other hand, the first term in (2.17) is unphysical, from the standpoint of (2.1). In summary then, our strategy should be to choose λ and c such that

$$|h_{tt}| \ll |c^2 h_{xx}| \ll |\lambda c_R h_x|. \tag{2.19}$$

Then, neglecting only the smallest term, (2.17) becomes

$$h_t + c_R(h)h_x = \frac{c^2}{\lambda} h_{xx}, \tag{2.20}$$

the diffusive form of (2.1). From (2.20), we see that for fixed Δx and Δt, and hence fixed c, λ controls the diffusion coefficient c^2/λ.

Suppose that $c_R(h)$ is nearly uniform, either because h is nearly uniform, or because $c_R(h)$ is a nearly constant function. Then since $h_t \approx c_R h_x$, we have $h_{tt} \approx c_R^2 h_{xx}$, and the first inequality in (2.19) corresponds to

$$c_R < c. \tag{2.21}$$

By (2.4), this is just the usual CLF criterion,

$$c_R < \frac{\Delta x}{\Delta t}, \tag{2.22}$$

that the physical wave cannot propagate farther than a lattice distance Δx in a time step Δt. If we include the effects of the first term in (2.17) (still assuming $h_t \approx c_R h_x$), then (2.20) becomes

$$h_t + c_R(h)h_x = \frac{c^2 - c_R^2}{\lambda} h_{xx}. \tag{2.23}$$

Thus, violation of the CLF criterion leads to instability in the form of a negative diffusion in (2.23).

The present example is an especially simple one. In more complicated cases, particularly those involving more than one space dimension, such a direct analysis of the full set of population equations becomes impractical. In these cases, it is better to use an approximation method—the Chapman-Enskog expansion—that explicitly tracks only the slow modes. Because it treats the more numerous fast modes only implicitly, the Chapman-

Enskog expansion can be carried to a higher order in Δt. This higher accuracy is important. For example, (2.20) suggests that the diffusion can be made arbitrarily small by making λ arbitrarily large, whereas general experience with equations like (2.3) leads us to expect that λ cannot be made much larger than about Δt^{-1}. Using the more accurate result of the Chapman-Enskog expansion, we find that the diffusion can indeed be made arbitrarily small, but by making λ close to the well-defined upper bound $2/\Delta t$. This insight proves critical for applications.

The Chapman-Enskog expansion is a *dual* expansion in Δt and in the nearness of each h_i to h_i^{eq}. The populations remain near their local equilibrium values because the decay parameter λ is large. Thus $\varepsilon \equiv 1/\lambda$ is the second small parameter. We assume that Δt and ε have the same small size, and we take the h_i^{eq} to be given by (2.18). Expanding (2.3) in Δt, we obtain

$$(D_i + \tfrac{1}{2}\Delta t D_i^2 + \cdots)h_i = -\lambda(h_i - h_i^{eq}), \qquad i = 1, 2 \tag{2.24}$$

where

$$D_1 = \frac{\partial}{\partial t} + c\frac{\partial}{\partial x} \qquad \text{and} \qquad D_2 = \frac{\partial}{\partial t} - c\frac{\partial}{\partial x}. \tag{2.25}$$

Then, expanding the h_i about their prescribed equilibrium values,

$$h_i = h_i^{eq} + \varepsilon h_i^{(1)} + \varepsilon^2 h_i^{(2)} + \cdots, \qquad \varepsilon \equiv \lambda^{-1}, \tag{2.26}$$

and substituting (2.26) into (2.24), we obtain

$$\left(D_i + \frac{1}{2}\Delta t D_i^2 + \cdots\right)(h_i^{eq} + \varepsilon h_i^{(1)} + \cdots) = -\frac{1}{\varepsilon}(\varepsilon h_i^{(1)} + \varepsilon^2 h_i^{(2)} + \cdots). \tag{2.27}$$

To the first two orders in Δt or ε, (2.27) takes the form

$$\Gamma_i^{(0)} + \Gamma_i^{(1)} = 0, \tag{2.28}$$

where

$$\Gamma_i^{(0)} = D_i h_i^{eq} + h_i^{(1)} \tag{2.29}$$

contains all the order one terms and

$$\Gamma_i^{(1)} = \tfrac{1}{2}\Delta t D_i^2 h_i^{eq} + \varepsilon D_i h_i^{(1)} + \varepsilon h_i^{(2)} \tag{2.30}$$

contains all the terms of order Δt or ε.

To get a closed equation for the slow mode $h(x, t)$, we sum (2.28) over i and use the conservation property (2.13) of (2.18), which implies that

$$\sum_i h_i^{(1)} = \sum_i h_i^{(2)} = \cdots = 0. \tag{2.31}$$

Thus, by (2.18),

$$\sum_i \Gamma_i^{(0)} = \sum_i D_i h_i^{eq} = \frac{\partial h}{\partial t} + c_R(h)\frac{\partial h}{\partial x}. \tag{2.32}$$

Similarly,

$$\sum_i \Gamma_i^{(1)} = \frac{1}{2}\Delta t \sum_i D_i^2 h_i^{eq} + \varepsilon \sum_i D_i h_i^{(1)}. \tag{2.33}$$

To consistent order, we may simplify (2.33) by substituting for $h_i^{(1)}$ from the leading order approximation to (2.28), namely

$$h_i^{(1)} = -D_i h_i^{eq}. \tag{2.34}$$

Thus, to consistent order,

$$\sum_i \Gamma_i^{(1)} = \frac{1}{2}\Delta t \sum_i D_i^2 h_i^{eq} - \varepsilon \sum_i D_i(D_i h_i^{eq}) = \left(\frac{\Delta t}{2} - \frac{1}{\lambda}\right)\sum_i D_i^2 h_i^{eq}. \tag{2.35}$$

Using (2.18) again, and the fact that $h_t = -c_R h_x$ at leading order, we find that, to consistent order,

$$\sum_i D_i^2 h_i^{eq} = h_{tt} + 2(c_R h_x)_t + c^2 h_{xx} \approx (c^2 - c_R^2)h_{xx}. \tag{2.36}$$

Thus, to the first two orders in Δt and ε, the Chapman-Enskog expansion yields

$$h_t + c_R(h)h_x = \left(\frac{1}{\lambda} - \frac{\Delta t}{2}\right)(c^2 - c_R^2)h_{xx}, \tag{2.37}$$

a more accurate version of (2.23). Once again, if c is much larger than c_R, then (2.37) becomes

$$h_t + c_R(h)h_x = \left(\frac{1}{\lambda} - \frac{\Delta t}{2}\right)c^2 h_{xx}. \tag{2.38}$$

Compare (2.38) to the corresponding but less accurate result (2.20). According to (2.38), the diffusion coefficient decreases with increasing λ, vanishing as λ approaches the critical value $2/\Delta t$. For still larger λ, the solutions of the LB equations become unstable.

3. The shallow-water equations

In this section we derive the LB approximation to the shallow water equations,

$$\frac{\partial h}{\partial t} + \frac{\partial}{\partial x_\alpha}(u_\alpha h) = 0 \tag{3.1}$$

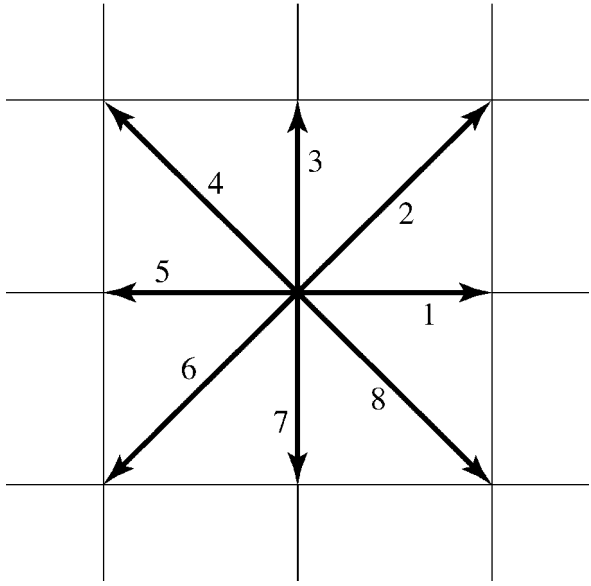

Figure 1. At each lattice point, particles move in one of 8 directions to an adjacent lattice point in a time step.

and

$$\frac{\partial}{\partial t}(u_\alpha h) + \frac{\partial}{\partial x_\beta} P_{\alpha\beta} = F_\alpha, \tag{3.2}$$

where

$$P_{\alpha\beta} = \tfrac{1}{2} g h^2 \delta_{\alpha\beta} + u_\alpha u_\beta h. \tag{3.3}$$

Here, h is the fluid depth, $(u_1, u_2) \equiv (u, v) \equiv \mathbf{u}$ is the fluid velocity, g is the gravity constant, and F_α is the sum of all the forces *including Coriolis force*. Repeated Greek subscripts are summed from 1 to 2.

We use a square two-dimensional lattice. Let Δx be the distance between lattice points in either direction. Refer to Figure 1. We adopt the 8-velocity model with

$$\mathbf{c}_0 = \mathbf{0} \tag{3.4}$$

for the velocity of the rest particle;

$$\mathbf{c}_1 = (c, 0), \qquad \mathbf{c}_3 = (0, c), \qquad \mathbf{c}_5 = (-c, 0), \qquad \mathbf{c}_7 = (0, -c) \tag{3.5}$$

for the velocities of the particles moving in the 4 coordinate directions; and

$$\mathbf{c}_2 = (c, c), \qquad \mathbf{c}_4 = (-c, c), \qquad \mathbf{c}_6 = (-c, -c), \qquad \mathbf{c}_8 = (c, -c) \tag{3.6}$$

for the particle velocities in the 4 diagonal directions. We take $c\Delta t = \Delta x$, so that all the particles (except the rest particle) move from lattice point to adjacent lattice point in a timestep Δt.

As in Section 2, we regard $h_i(\mathbf{x}, t)$ as the population of particles with velocity $\mathbf{c}_i$ at lattice point $\mathbf{x}$ and time t. The equations

$$h(\mathbf{x}, t) = \sum_{i=0}^{8} h_i(\mathbf{x}, t) \tag{3.7}$$

and

$$h\mathbf{u}(\mathbf{x}, t) = \sum_{i=0}^{8} \mathbf{c}_i h_i(\mathbf{x}, t) \tag{3.8}$$

relate the 9 populations $\{h_i(\mathbf{x}, t),\ i = 0, 8\}$ at lattice point $\mathbf{x}$ and time t to the fluid depth $h(\mathbf{x}, t)$ and velocity $\mathbf{u}(\mathbf{x}, t)$ at the same location and time. Since $\mathbf{c}_0 = \mathbf{0}$, the rest particles do not contribute to the momentum. The three physical variables h, u, and v are the slow modes of the LB model. Thus there are $9 - 3 = 6$ fast modes.

Once again, the LB dynamics comprises two steps: a collision step, which adjusts the populations at each lattice point, followed by a streaming step, in which particles move to the neighboring lattice points. The collision step is governed by

$$h_i'(\mathbf{x}, t) = h_i(\mathbf{x}, t) - \lambda\Delta t(h_i(\mathbf{x}, t) - h_i^{eq}(\mathbf{x}, t)) \tag{3.9}$$

where λ is the decay coefficient, and the prime denotes the value immediately after the collision. The equilibrium populations

$$h^{eq}(\mathbf{x}) \equiv \{h_0^{eq}(\mathbf{x}), h_1^{eq}(\mathbf{x}), \ldots, h_8^{eq}(\mathbf{x})\} \tag{3.10}$$

remain to be defined. The streaming step is governed by

$$h_i(\mathbf{x} + \mathbf{c}_i\Delta t, t + \Delta t) + h_i'(\mathbf{x}, t) + \frac{\Delta t}{6c^2} c_{i\alpha}\left(\frac{1}{2} F_\alpha(\mathbf{x}, t) + \frac{1}{2} F_\alpha(\mathbf{x} + \mathbf{c}_i\Delta t, t + \Delta t)\right) \tag{3.11}$$

where $c_{i\alpha}$ is the component of $\mathbf{c}_i$ in the α-direction. Once again, repeated Greek indices are summed. Note that the forcing term in (3.11) represents an average of the values at the departure point $(\mathbf{x}, t)$ and the arrival point $(\mathbf{x} + \mathbf{c}_i\Delta t, t + \Delta t)$ of the streaming particle; this proves essential to maintaining second order accuracy in the Chapman-Enskog expansion. Combining (3.9) and (3.11) into a single formula, we obtain the complete LB dynamics

$$\begin{aligned} h_i(\mathbf{x} + \mathbf{c}_i\Delta t, t + \Delta t) - h_i(\mathbf{x}, t) - \frac{\Delta t}{6c^2} c_{i\alpha}\left(\frac{1}{2} F_\alpha(\mathbf{x}, t) + \frac{1}{2} F_\alpha(\mathbf{x} + \mathbf{c}_i\Delta t, t + \Delta t)\right) \\ = -\lambda\Delta t(h_i(\mathbf{x}, t) - h_i^{eq}(\mathbf{x}, t)). \end{aligned} \tag{3.12}$$

Once again, our strategy is to choose the constants c, Δt, and λ, and the 9 functions

$h_i^{eq}(h, u, v)$ (where h, u, v are defined by (3.6–8)) such that the slow modes computed from (3.12) approximately satisfy the shallow water equations. The choices

$$h_0^{eq} = h - \frac{5gh^2}{6c^2} - \frac{2h}{3c^2}\,\mathbf{u}\cdot\mathbf{u} \tag{3.13}$$

$$h_i^{eq} = \frac{gh^2}{6c^2} + \frac{h}{3c^2}\,c_{i\alpha}u_a + \frac{h}{2c^4}\,c_{i\alpha}c_{i\beta}u_\alpha u_\beta - \frac{h}{6c^2}\,\mathbf{u}\cdot\mathbf{u}, \qquad \text{odd } i \tag{3.14}$$

$$h_i^{eq} = \frac{gh^2}{24c^2} + \frac{h}{12c^2}\,c_{i\alpha}u_\alpha + \frac{h}{8c^4}\,c_{i\alpha}c_{i\beta}u_\alpha u_\beta - \frac{h}{24c^2}\,\mathbf{u}\cdot\mathbf{u}, \qquad \text{even } i \tag{3.15}$$

have the important properties that

$$\sum_i h_i^{eq} = h, \tag{3.16}$$

$$\sum_i c_{i\alpha} h_i^{eq} = hu_\alpha, \tag{3.17}$$

and

$$\sum_i c_{i\alpha}c_{i\beta}h_i^{eq} = \frac{1}{2}\,gh^2\delta_{\alpha\beta} + u_\alpha u_\beta h. \tag{3.18}$$

As always, the equilibrium populations h_i^{eq} depend only on the slow modes h, u, and v. The specific choices (3.13–15) are somewhat arbitrary, but we shall see that the properties (3.16–18) guarantee that the slow mode dynamics approximates the shallow-water equations (3.1–3). The properties (3.16) and (3.17) correspond to the conservation of mass and momentum, respectively, by the collisions (3.9). Property (3.18) makes the momentum flux of the LB particles equal to the momentum flux (3.3) of the shallow water equations. For a motivated derivation of (3.13–15), see the Appendix.

The LB dynamics (3.12) comprises 9 evolution equations for the 9 population variables h_i. Because there are so many dependent variables, a direct analysis of the full set of equations like that performed in Section 2 is rather difficult. However, most of the dependent variables represent fast modes. Therefore, the Chapman-Enskog expansion, which pursues only the slow modes, remains relatively easy. Once again, the Chapman-Enskog expansion is a dual expansion in Δt and $\varepsilon \equiv \lambda^{-1}$, which are assumed to be of the same order. The smallness of Δt (for fixed c) corresponds to the assumption that the population variables vary slowly on the scale of the lattice spacing and the time step. The smallness of ε corresponds to the assumption that the collisions hold the populations near their equilibrium values (3.13–15). Expanding (3.12) in Δt, and substituting

$$h_i = h_i^{eq} + \varepsilon h_i^{(1)} + \varepsilon^2 h_i^{(2)} + \cdots \tag{3.19}$$

we obtain

$$\left(D_i + \frac{1}{2}\Delta t\, D_i^2 + \cdots\right)(h_i^{eq} + \varepsilon h_i^{(1)} + \cdots) - \frac{1}{6c^2}\, c_{i\alpha}\left(1 + \frac{1}{2}\Delta t\, D_i + \cdots\right)F_\alpha(\mathbf{x}, t) = -\frac{1}{\varepsilon}(\varepsilon h_i^{(1)} + \varepsilon^2 h_i^{(2)} + \cdots) \tag{3.20}$$

where

$$D_i \equiv \frac{\partial}{\partial t} + c_{i\alpha}\frac{\partial}{\partial x_\alpha}. \tag{3.21}$$

To the first two orders in ε or Δt, (3.20) is

$$\Gamma_i^{(0)} + \Gamma_i^{(1)} = 0, \tag{3.22}$$

where

$$\Gamma_i^{(0)} = D_i h_i^{eq} - \frac{1}{6c^2}\, c_{i\alpha}F_\alpha + h_i^{(1)} \tag{3.23}$$

contains the order one terms, and

$$\Gamma_i^{(1)} = \frac{1}{2}\Delta t D_i^2 h_i^{eq} + \varepsilon D_i h_i^{(1)} - \frac{\Delta t}{12c^2}\, c_{i\alpha}D_i F_\alpha + \varepsilon h_i^{(2)} \tag{3.24}$$

contains the terms of order Δt or ε. As in Section 2, we may consistently use the leading order balance in (3.22) to simplify the next order terms. Thus solving $\Gamma_i^{(0)} = 0$ for $D_i h_i^{eq}$ and substituting the result into (3.24) yields

$$\Gamma_i^{(1)} \approx \left(\varepsilon - \frac{\Delta t}{2}\right)D_i h_i^{(1)} + \varepsilon h_i^{(2)}. \tag{3.25}$$

To obtain the slow mode dynamics, we apply $\sum_i$ and $\sum_i c_{i\alpha}$ to (3.22). Since the h^{eq} defined by (3.13–15) satisfy (3.16) and (3.17), it follows from (3.19) that

$$\sum_i h_i^{(1)} = \sum_i h_i^{(2)} = \sum_i c_{i\alpha}h_i^{(1)} = \sum_i c_{i\alpha}h_i^{(2)} = 0. \tag{3.26}$$

Therefore (3.23) implies that

$$\sum_i \Gamma_i^{(0)} = \sum_i D_i h_i^{eq} = \frac{\partial h}{\partial t} + \frac{\partial}{\partial x_\alpha}(hu_\alpha), \tag{3.27}$$

and (3.25) implies that

$$\sum_i \Gamma_i^{(1)} = 0. \tag{3.28}$$

Thus the LB dynamics implies the shallow water continuity equation (3.1) with an acuracy of $O(\varepsilon^2)$.

To obtain the corresponding momentum equation, we use (3.23), (3.26) and (3.16–18) to compute

$$\sum_i c_{i\alpha}\Gamma_i^{(0)} = \frac{\partial}{\partial t}(u_\alpha h) + \frac{\partial}{\partial x_\beta} P_{\alpha\beta} - F_\alpha, \tag{3.29}$$

where $P_{\alpha\beta}$ is given by (3.3). Similarly, from (3.25) we obtain

$$\sum_i c_{i\alpha}\Gamma_i^{(1)} = \left(\varepsilon - \frac{\Delta t}{2}\right)\frac{\partial}{\partial x_\beta}\sum_i c_{i\alpha}c_{i\beta}h_i^{(1)}. \tag{3.30}$$

Thus, with an accuracy of $O(\varepsilon^2)$, the LB dynamics implies

$$\frac{\partial}{\partial t}(u_\alpha h) + \frac{\partial}{\partial x_\beta} P_{\alpha\beta} - F_\alpha = -\frac{\partial}{\partial x_\beta} T_{\alpha\beta} \tag{3.31}$$

where the viscous tensor

$$T_{\alpha\beta} = \left(\varepsilon - \frac{\Delta t}{2}\right)\sum_i c_{i\alpha}c_{i\beta}h_i^{(1)} \tag{3.32}$$

represents the higher order terms. To consistent order, we may substitute the leading order balance

$$h_i^{(1)} = -D_i h_i^{eq} + \frac{1}{6c^2} c_{i\alpha}F_\alpha \tag{3.33}$$

into the higher order term (3.32). We obtain

$$T_{\alpha\beta} = \left(\frac{\Delta t}{2} - \varepsilon\right)\left(\frac{\partial}{\partial t}\sum_i c_{i\alpha}c_{i\beta}h_i^{eq} + \frac{\partial}{\partial x_\gamma}\sum_i c_{i\alpha}c_{i\beta}c_{i\gamma}h_i^{eq}\right). \tag{3.34}$$

If we choose $c^2 \gg gh$—the analog of $c \gg c_R$ in Section 2—then the contribution of the $\partial/\partial t$-term in (3.34) is negligible. Using (3.14–15) to evaluate the other term, we obtain

$$T_{\alpha\beta} = \left(\frac{\Delta t}{2} - \varepsilon\right)\frac{1}{3}c^2\left\{\nabla\cdot(h\mathbf{u})\delta_{\alpha\beta} + \frac{\partial}{\partial x_\alpha}(hu_\beta) + \frac{\partial}{\partial x_\beta}(hu_\alpha)\right\}. \tag{3.35}$$

Thus

$$\frac{\partial T_{\alpha\beta}}{\partial x_\beta} = \left(\frac{\Delta t}{2} - \varepsilon\right)\frac{1}{3}c^2\left\{2\frac{\partial}{\partial x_\alpha}\nabla\cdot(h\mathbf{u}) + \frac{\partial^2}{\partial x_\beta \partial x_\beta}(hu_\alpha)\right\}. \tag{3.36}$$

The first term in the curly bracket represents a small correction to the pressure; the second term resembles the usual viscosity. If we retain only this second term, then (3.31) becomes

$$\frac{\partial}{\partial t}(u_\alpha h) + \frac{\partial}{\partial x_\beta} P_{\alpha\beta} - F_\alpha = \nu \frac{\partial^2 (h u_\alpha)}{\partial x_\beta \partial x_\beta} \tag{3.37}$$

where

$$\nu = \frac{1}{3} c^2 \left\{ \frac{1}{\lambda} - \frac{\Delta t}{2} \right\} \tag{3.38}$$

is the viscosity coefficient. Thus, to the second order in ε and Δt, the LB dynamics implies the continuity equation (3.1) and the momentum equation (3.37) with viscosity coefficient (3.38).

We conclude this section by summarizing the shallow water LB model as an algorithm with a 4-step cycle:

(1) Given the populations $h_i(\mathbf{x}, t)$ at every lattice point $\mathbf{x}$, compute the fluid depth and velocity from (3.7–8).

(2) From these $h(\mathbf{x})$ and $\mathbf{u}(\mathbf{x})$, compute the equilibrium populations $h_i^{eq}(\mathbf{x}, t)$ from (3.13–15).

(3) Collide the particles using (3.9).

(4) Stream the particles using (3.11). Return to step (1).

Once again, to the first two orders of approximation, this algorithm is equivalent to the viscous shallow-water dynamics (3.1) and (3.37–38).

4. Numerical experiments

We consider an ocean composed of two immiscible layers with different uniform mass densities, and we assume that the lower layer is at rest. The upper layer is governed by the shallow water equations with *reduced* gravity g. For these we use the LB model derived in Section 3, with forcing

$$F_\alpha = \varepsilon_{\alpha\beta} f h u_\beta + \frac{h}{h + \delta_E} \tau_\alpha. \tag{4.1}$$

Here, $\varepsilon_{\alpha\beta}$ is the permutation symbol, $f = f_0 + \beta y$ is the Coriolis parameter, $\tau(x, y) = (\tau_1, \tau_2)$ is the prescribed wind stress (divided by 1 gm cm^{-3}), and δ_E is the *Ekman thickness,* a prescribed constant. By the results of Section 3, solutions of the LB equations with forcing (4.1) approximately satisfy

$$(h\mathbf{u})_t + (hu\mathbf{u})_x + (hv\mathbf{u})_y + f\mathbf{k} \times h\mathbf{u} = -gh\nabla h + \frac{h}{h + \delta_E} \tau + \nu \nabla^2 (h\mathbf{u}) \tag{4.2}$$

and

$$\frac{\partial h}{\partial t} + \nabla \cdot (h\mathbf{u}) = 0, \tag{4.3}$$

where $\nabla = (\partial_x, \partial_y)$ and

$$\nu = \left(\frac{1}{\lambda} - \frac{1}{\lambda_{max}}\right)\frac{c^2}{3}, \tag{4.4}$$

with $\lambda_{max} = 2/\Delta t$ and $c = \Delta x/\Delta t$ as before.

Models like (4.2–3), often called *one-and-one-half layer models* or *reduced gravity models,* are frequently studied prototypes for the more complex multi-layer or continuously stratified ocean circulation models. The atypical features of (4.2) are the quotient preceding the wind stress, and the presence, inside the viscous Laplacian, of the factor h. The latter is a typical feature of LB calculations, an example of the "inflexibility" mentioned in Section 1. If $\mathbf{u}$ varies on a smaller lengthscale than h, then the viscosity in (4.2) is practically the same as standard Navier-Stokes viscosity. However, in the present application, there is no compelling reason to prefer one form of viscosity over the other. It is even conceivable that the dissipation operator in (4.2), which arises naturally from the collide-and-stream algorithm, may have advantages over more arbitrarily chosen dissipation operators. Of course, one could turn off the viscosity in (4.2) by setting $\lambda = \lambda_{max}$, and then insert a completely arbitrary dissipation into the forcing F_α. However, that would violate the aesthetic principle that LB dynamics should be based on the simplest feasible set of operations.

As for the quotient in the wind forcing term, we imagine that all of the momentum put in by the wind stress is mixed downward through an "Ekman layer" of depth δ_E by small-scale processes not contained in the model. If the upper layer depth h is much greater than δ_E, then the quotient in (4.1) is near unity, and the upper layer absorbs nearly all of the momentum put in by the wind. However, if $h < \delta_E$ then the upper layer absorbs only a fraction, h/δ_E, of the wind momentum; the rest is lost to the lower layer, which nevertheless remains at rest because of its great presumed thickness. This forcing strategy, which can be viewed as an alternative to interfacial friction, avoids the unrealistic behavior that could develop if a finite amount of wind mometum were spread over a vanishing upper layer depth. In all the solutions discussed, $\delta_E = 100$ m.

We solve (4.2–3) in the square box, $0 < x, y < L = 4000$ km. All the solutions discussed have 100 lattice points in each direction. Thus $\Delta x = 40$ km. The reduced gravity has the value $g = .002 \times 9.8$ m sec^{-2}. For an upper layer depth of $h = 500$ m, this corresponds to an internal gravity wave speed $(gh)^{1/2}$ of 270 km day^{-1}. We choose $c = 540$ km day^{-1} to fulfill the CLF criterion that c be larger than the speed of the gravity waves, the fastest waves present in the shallow water equations. Then $\Delta t = \Delta x/c = .075$ day. We take $f_0 = 2\pi$ day^{-1} and $\beta = f_0/6400$ km. For $h = 500$ m, this corresponds to an internal deformation

radius $(gh)^{1/2}/f_0$ of 43 km, and an internal Rossby wave speed $gh\beta/f_0^2$ of 1.8 km day^{-1}, at the southern boundary. At this speed, Rossy waves cross the basin in about 6 years.

In all the experiments discussed, $\tau_y = 0$, and

$$\tau_x = \sin^2(\pi y/L) \text{ dyn cm}^{-2}. \tag{4.5}$$

Thus the wind blows west to east with a maximum force at mid-latitude, and both the wind stress and its curl vanish at the northern and southern boundaries. The anticipated circulation has two gyres.

The relaxation coefficient λ controls the viscosity ν. Since λ is of order Δt^{-1}, the viscosity ν has scale size $c^2\Delta t = c\Delta x = 25 \times 10^8$ cm^2 sec^{-1}. This corresponds to a Munk boundary layer thickness $\delta_M \equiv (\nu/\beta)^{1/3}$ of 280 km, which is too large. Realistically small viscosity relies on the cancellation between terms in (4.4) as $\lambda \to \lambda_{max}$. In all of the experiments discussed, $\lambda = 0.95 \times \lambda_{max}$ corresponding to $\nu = 0.033\, c\Delta x$ and $\delta_M = 90$ km, about 2 lattice spacings. The ability to reduce the viscosity by choosing λ very close to λ_{max} is absolutely vital for the practical application of LB methods. Otherwise the high intrinsic viscosity of LB dynamics makes the solutions unrealistically diffusive. Recall that the λ_{max}-term in (4.4) arises from a second order term in Δt in the Chapman-Enskog expansion.

The streaming step (3.11) requires the forcing $F_\alpha(\mathbf{x} + \mathbf{c}_i\Delta t, t + \Delta t)$ at the particle destination and the new time. Since the forcing (4.1) involves the depth and velocity (which depend on the h_i), (3.11) is an implicit equation for h_i at the new time. We solve (3.11) using a predictor-corrector method. In the predictor, we evaluate both forcing terms in (3.11) at the departure location and time. In each corrector, we evaluate the forcing term at the destination by using the previous iterate. Although 1 or 2 correctors seemed sufficient, all the solutions discussed use 4 correctors. The need for a predictor/corrector method to accommodate the Coriolis force somewhat compromises the efficiency and aesthetics of the LB model.

We consider all of the lattice points to lie within the fluid. The collision step is the same at all lattice points. At the lattice points closest to the boundary, we modify the streaming step (3.11) to incorporate the boundary conditions. All the experiments discussed used one of two algorithms. In the algorithm corresponding to *no stress,* particles streaming toward the boundary experience elastic collisions, as shown in Figure 2a. In the algorithm corresponding to *no slip,* particles streaming toward the boundary bounce back in the direction from which they came, as shown in Figure 2b. Both of these algorithms are standard methodology in applications of LB dynamics. Note that, in both cases, the boundary lies one half lattice distance outside the last row of lattice points. Apart from the interaction with the boundary (that is, as regards the evaluation of the forcing terms and the use of predictor-corrector), the streaming step is the same at all lattice points.

Parsons (1969) and especially Veronis (1973, 1980) developed a relatively complete theory of wind-driven, reduced-gravity flow based upon *planetary geostrophic dynamics,* in which the inertia $D\mathbf{u}/Dt$ is omitted from the shallow water momentum equation. For a brief summary of their theory, see Salmon (1998a, pp. 182–188). To investigate planetary

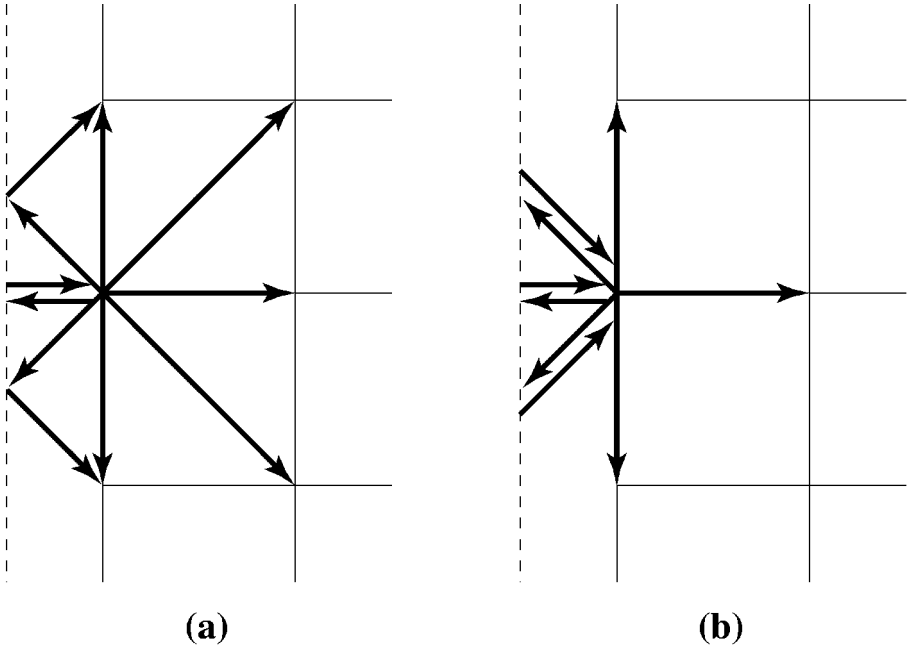

Figure 2. The streaming of particles from a lattice point near the boundary. The boundary is dashed. (a) Elastic collisions with the boundary correspond to the boundary condition of no stress, that is, no normal transport of tangential momentum. (b) So-called "bounce back" collisions correspond to no-slip boundary conditions.

geostrophic dynamics, we note that if all the terms quadratic in the velocity are simply dropped from the equilibrium populations (3.13–15), then the Chapman-Enskog expansion yields the same continuity equation (4.3) as before. However, the resulting momentum equation,

$$(h\mathbf{u})_t + f\mathbf{k} \times h\mathbf{u} = -gh\nabla h + \frac{h}{h + \delta_E}\tau + \nu\nabla^2(h\mathbf{u}), \tag{4.6}$$

contains the local time derivative of the velocity, but omits the advection of momentum. Our calculations show that the LB solutions of (4.3) and (4.6) with steady wind forcing always eventually become steady. Thus, by simply dropping the $O(\mathbf{u}^2)$ terms in (3.13–15) we eventually obtain solutions of the planetary geostrophic equations in the form (4.3) and

$$f\mathbf{k} \times h\mathbf{u} = -gh\nabla h + \frac{h}{h + \delta_E}\tau + \nu\nabla^2(h\mathbf{u}) \tag{4.7}$$

Figures 3 and 4 depict LB solutions of the shallow water (SW) and planetary geostrophic (PG) equations using the forcing and parameter settings just described. All solutions begin from a state of rest with uniform upper layer depth h. The solutions differ only in their

dynamics (SW or PG), their boundary conditions (no slip or no stress), and in the total volume of upper layer water. If the upper layer volume is sufficiently small, then, according to the theory of Veronis, the wind stress (4.5) produces a northeastward flowing *separated* western boundary current (like the North Atlantic Current) and a southward flowing *isolated* western boundary current (like the Labrador Current). Between these two currents, the motionless lower layer outcrops at the sea surface. All the solutions of Figure 3 have an upper layer volume equivalent to an average h of 500 m. This is just above the critical value for which lower layer outcropping occurs. In contrast, all the solutions of Figure 4 have a mean layer depth of 300 m. For this lower volume of upper layer water, the lower layer outcrops over a broad area in the northern gyre. The outcrop region is in fact a region of small but nonvanishing h maintained by the requirement that h remain greater than 5 m. If, at any lattice point, h falls below 5 m, upper layer water is added to make $h = 5$ m. Without this simple augmentation, the LB algorithm described in Section 3 eventually becomes unstable for the solutions in which h vanishes.

Table 1 summarizes all of the numerical solutions discussed. The "years" column gives the duration of the experiment in simulated years. All of the solutions became steady or statistically steady after about two decades, but some were run much longer to check for stationarity or to investigate small trends. The h-column in Table 1 gives the range of upper layer depth in the corresponding figure. The $|h\mathbf{u}|$-column gives the maximum transport, in Sverdrups per kilometer distance in the direction normal to $\mathbf{u}$. (1 Sverdrup = 1 Sv = 10^6 m^3 sec^{-1}.) This maximum transport corresponds to the longest arrow in the corresponding figure and thus sets the scale for the arrows. The last column in Table 1 gives the total transport of the southern (northern) gyre in Sverdrups. The northern transport approaches the southern transport only in the cases where $h > \delta_E$ over most of the northern gyre, that is, only in the experiments with the greater upper layer volume.

In every case, the SW solutions remain unsteady, but approach statistically steady states that are well established by the times given in Table 1 and shown in the figures. The fluctuations about the mean are largest in the two SW solutions with the deeper upper layer (Fig. 3a–b), which feel the full wind forcing over a greater fraction of the domain. However, even in the SW no-slip solution of Figure 3a, which exhibited the largest fluctuations, the depth and velocity fields shown on the figure closely resemble those in many other snapshots taken at different times. The two SW solutions with the shallower upper layer (Fig. 4a–b) exhibited very small fluctuations, and could be described as quasi-steady.

In contrast, the PG solutions, corresponding to the LB equivalent of (4.3, 4.6), always eventually become steady; hence we may consider them as solutions of (4.3, 4.7). The PG solutions lack the quasi-stationary meanders and large inertial recirculations of the SW solutions near the western boundary. However, the corresponding SW and PG solutions generally resemble one another, especially in the ocean interior. Overall, the PG solutions could be described as everywhere laminar and therefore somewhat less interesting than the corresponding SW solutions.

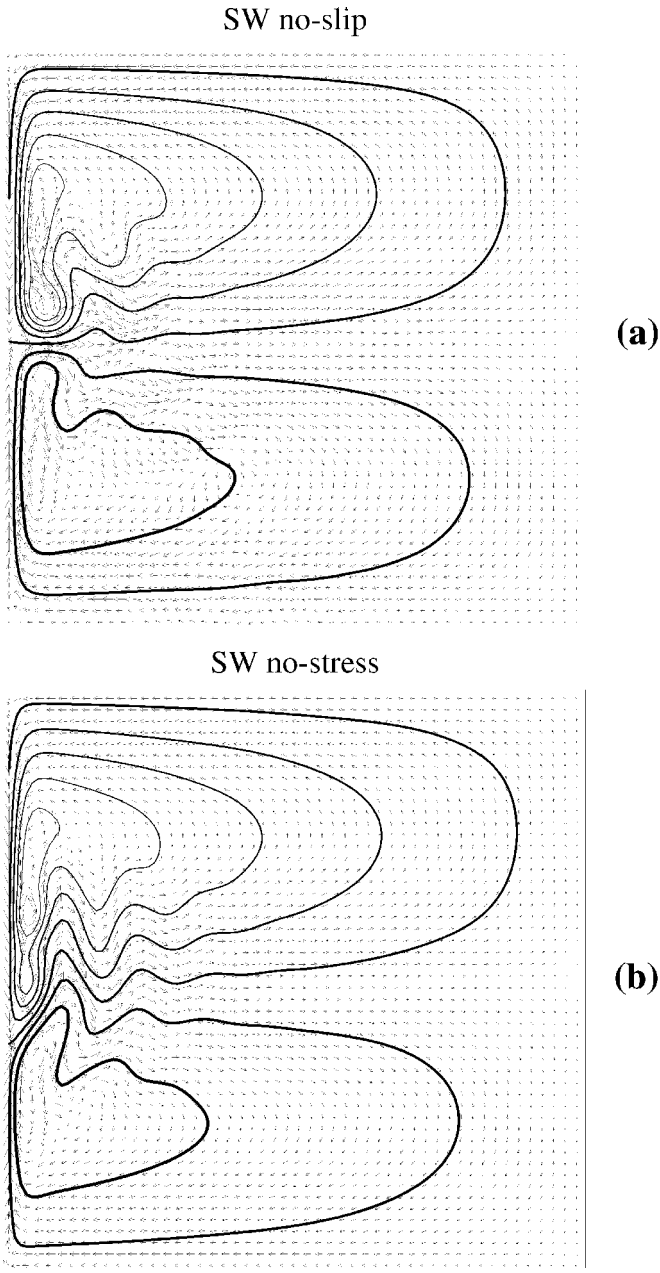

Figure 3. Numerical solutions of the reduced gravity model using the 8-velocity lattice Boltzmann method described in Sections 3 and 4. All 4 solutions correspond to an average layer depth of 500 m. Contours represent the layer depth h, with darker contours corresponding to larger h. See Table 1 for the range of h in each picture. Arrows represent the transport $h\mathbf{u}$, with the length of each arrow proportional to the *square root* of the transport (to reduce the range of arrow sizes). The longest arrow corresponds to the maximum transport given in Table 1. (a) Shallow water dynamics with no-slip boundary conditions. (b) Shallow water dynamics with no-stress boundary conditions. (c) Planetary geostrophic dynamics with no-slip boundary conditions. (d) Planetary geostrophic dynamics with no-stress boundary conditions.

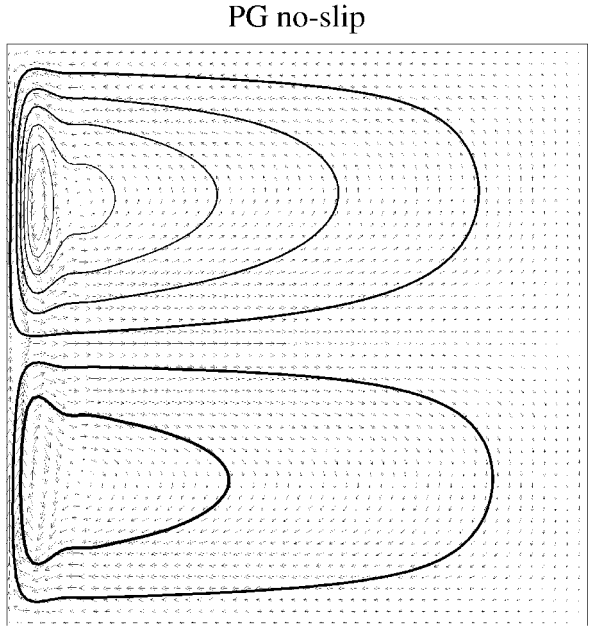

(c)

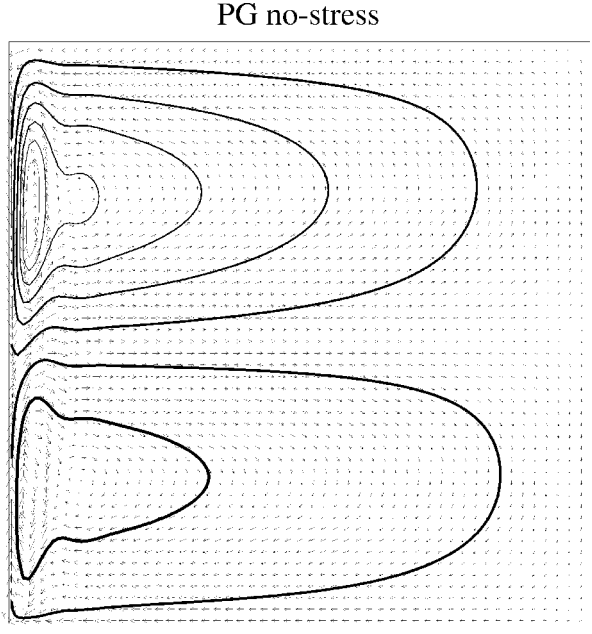

(d)

Figure 3. (Continued)

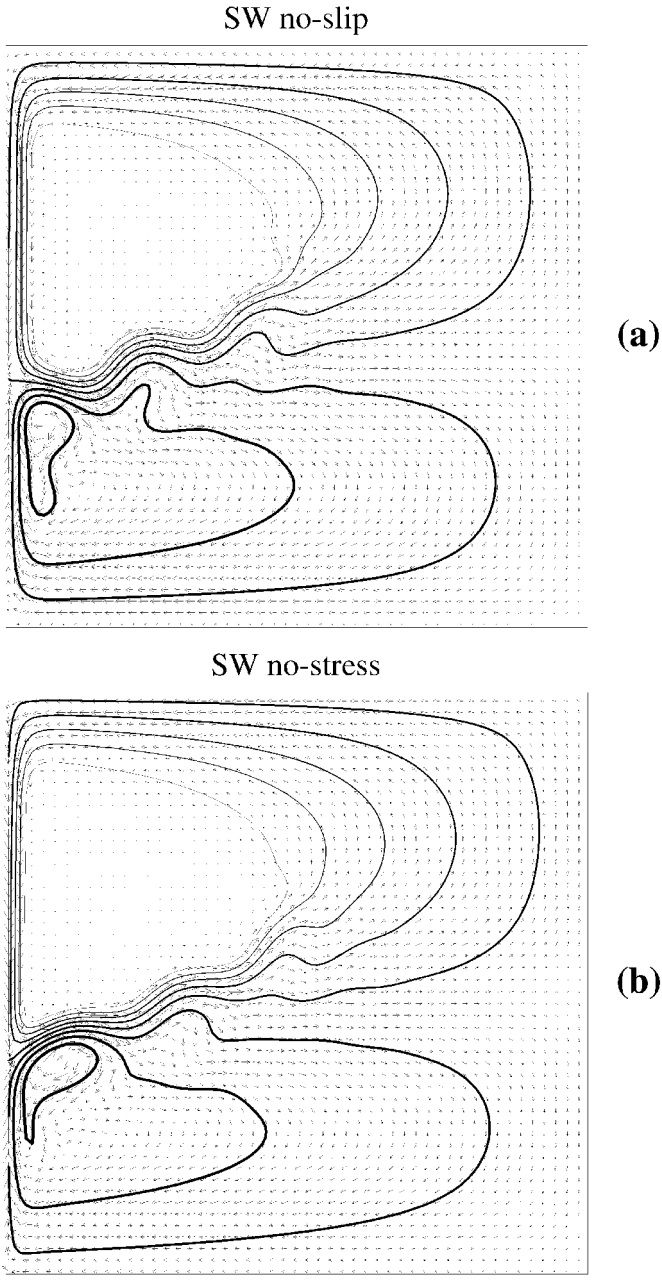

Figure 4. The same as Figure 3, but for an average layer depth of 300 m. At this lower volume of upper layer water, the motionless lower layer outcrops over a broad area in the northern gyre.

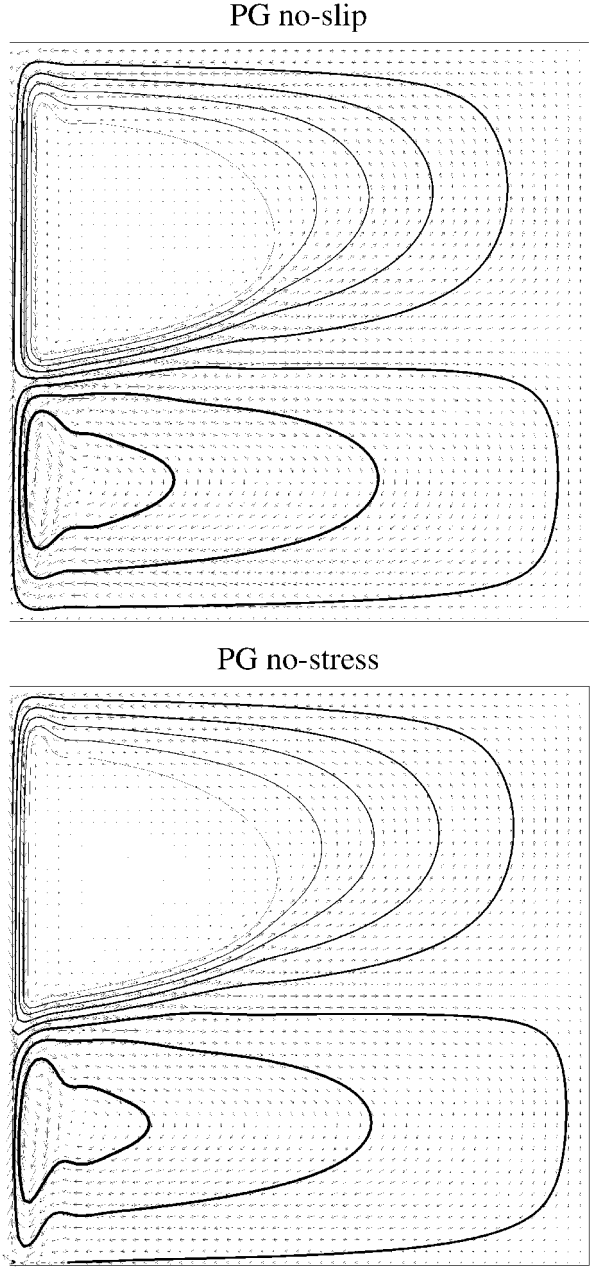

Figure 4. (Continued)

Table 1. Summary of numerical experiments.

Fig.	Dynamics	Average h	B. cond.	Years	h min (max)	Maximum $\lvert h\mathbf{u}\rvert$	s (n) gyre transports
3a	SW	500 m	no-slip	40	100m (687 m)	0.20 Sv km^{-1}	25.3 Sv (22.4 Sv)
3b	SW	500	no-stress	60	87 (697)	0.30	26.4 (23.8)
3c	PG	500	no-slip	30	44 (695)	0.20	26.4 (24.0)
3d	PG	500	no-stress	60	5 (710)	0.33	28.7 (24.6)
4a	SW	300 m	no-slip	55	5 (582)	0.17	25.6 (11.3)
4b	SW	300	no-stress	85	5 (597)	0.22	26.9 (11.9)
4c	PG	300	no-slip	40	5 (550)	0.17	21.9 (11.3)
4d	PG	300	no-stress	40	5 (560)	0.26	22.7 (11.9)
6a	PG-4	500 m	no-normal	40	173 (674)	0.41	22.7 (21.2)
6b	PG-4	300 m	flow	60	5 (531)	0.31	19.3 (11.3)

Like the full shallow water equations (4.2–3), the system (4.3, 4.6) contains inertia-gravity waves; the linearized approximations to both systems are identical. Thus, both systems contain the same number of fast and slow modes, and both systems demand about the same amount of computation. (Because of the need for predictor/corrector, the streaming step uses the most processor time, so the time saved by not calculating the $O(\mathbf{u}^2)$ terms in (3.13–15) is relatively insignificant.) Beyond the comparison between SW and PG solutions, what then is gained by throwing out the momentum advection?

5. The 4-velocity model

I believe there are two advantages to the omission of momentum advection. One advantage has a physical basis; the other is computational. Both advantages are likely to be much more significant in three dimensions than in two dimensions, but it is worthwhile to consider them here. We consider the physical advantage of PG in the following section and devote this section to the computational advantage.

The computational advantage of (4.6) arises from the fact that the corresponding LB model requires only 4 nonzero velocities at each lattice point. Refer to Figure 5a. Including the rest particle, this *4-velocity model* contains only 5 (instead of 9) modes, and only 2 of the 5 modes are fast modes in the sense of Section 2.

The 4-velocity model of Figure 5 *cannot* be used for the physics (3.13–15) containing momentum advection, because its lower degree of isotropy leads to a completely incorrect representation of the momentum flux tensor.[2] For example, it is intuitively obvious that the 4-velocity model cannot represent the northward advection of eastward momentum because the 4-velocity model lacks diagonal links; the northward moving particles have no eastward momentum, and vice versa. In the full shallow water equations, this deficiency is associated with the existence of spurious *line invariants,* that is, with the conservation, in

2. The need for a lattice with sufficient symmetry to represent the desired physics was first recognized by Frisch *et al.* (1986); their classic paper inspired much of the subsequent interest in lattice gases and related methods like LB.

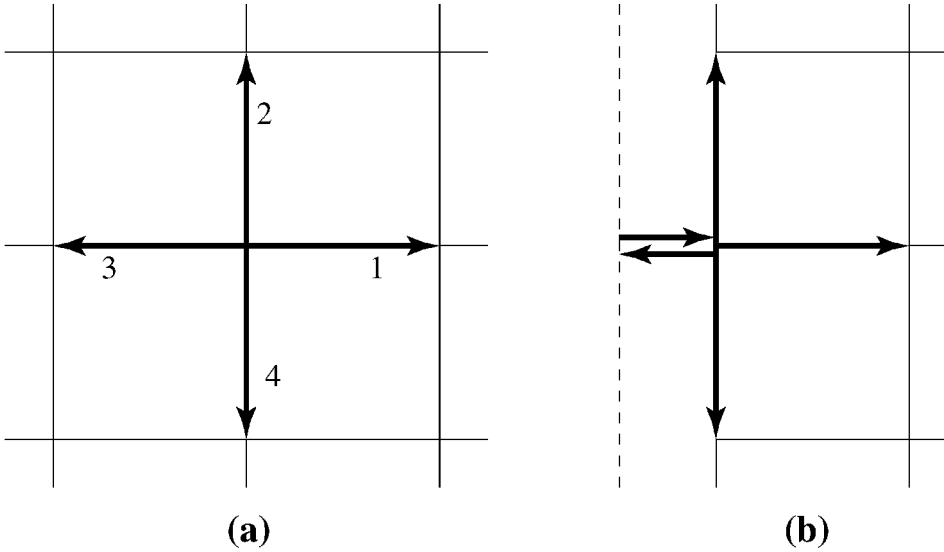

Figure 5. (a) In the 4-velocity model, particles move only in the 4 coordinate directions. (b) Only particles moving in the normal direction collide with the boundary.

unbounded flow, of the momentum along each lattice row and column. However, when, as in the planetary geostrophic equations, we neglect the momentum advection *a priori* and drop the corresponding terms in (3.13–15), then the symmetry of the 4-velocity model proves *nearly* sufficient to yield isotropic equations for the fluid. The remaining subtlety involves the viscosity.

In the 4-velocity model, the 4 moving particles move in the 4 coordinate directions with velocities

$$\mathbf{c}_1 = (c, 0), \qquad \mathbf{c}_2 = (0, c), \qquad \mathbf{c}_3 = (-c, 0), \qquad \mathbf{c}_4 = (0, -c). \tag{5.1}$$

Refer again to Figure 5. The LB dynamics, analogous to (3.12), is

$$h_i(\mathbf{x} + \mathbf{c}_i\Delta t, t + \Delta t) - h_i(\mathbf{x}, t) - \frac{\Delta t}{2c^2} c_{i\alpha}\left(\frac{1}{2}F_\alpha(\mathbf{x}, t) + \frac{1}{2}F_\alpha(\mathbf{x} + \mathbf{c}_i\Delta t, t + \Delta t)\right) = -\lambda\Delta t(h_i(\mathbf{x}, t) - h_i^{eq}(\mathbf{x}, t)). \tag{5.2}$$

Now, however, the equilibrium populations are given by

$$h_0^{eq} = h - \frac{gh^2}{c^2}$$
$$h_i^{eq} = \frac{gh^2}{4c^2} + \frac{h}{2c^2} c_{i\alpha}u_\alpha, \qquad i \neq 0, \tag{5.3}$$

which contain no $O(\mathbf{u}^2)$ terms. The equilibrium populations (5.3) satisfy (3.16), (3.17), and

$$\sum_i c_{i\alpha} c_{i\beta} h_i^{eq} = \frac{1}{2} g h^2 \delta_{\alpha\beta}, \tag{5.4}$$

the analog of (3.18).

Once again, we may use the Chapman-Enskog expansion to derive equations for the slow modes. However, because the 4-velocity model contains only 2 fast modes, it is more interesting to follow the first of the two methods illustrated in Section 2—the expansion in Δt alone. To the first order in Δt, (5.2) implies

$$\left(\frac{\partial}{\partial t} + c_{i\alpha} \frac{\partial}{\partial x_\alpha}\right) h_i = \frac{1}{2c^2} c_{i\alpha} F_\alpha - \lambda (h_i - h_i^{eq}). \tag{5.5}$$

As usual, we obtain the slow mode equations from the weighted sums of (5.5). Summing (5.5) from $i = 0$ to 4 yields the continuity equation (4.3); summing $c_{i\alpha}$ times (5.5) yields the momentum equation

$$\frac{\partial}{\partial t}(h u_\alpha) + \frac{\partial R_{\alpha\beta}}{\partial x_\beta} = F_\alpha, \tag{5.6}$$

where

$$R_{\alpha\beta} \equiv \sum_i c_{i\alpha} c_{i\beta} h_i \tag{5.7}$$

and F_α is given by (4.1). At equilibrium, (5.7) takes the value (5.4); as in Section 3, the difference between (5.7) and (5.4) is the viscous tensor. In the 4-velocity model,

$$R_{11} = c^2(h_1 + h_3), \qquad R_{22} = c^2(h_2 + h_4), \qquad R_{12} = R_{21} = 0. \tag{5.8}$$

Thus it is convenient to take R_{11} and R_{22} as the remaining two (fast) modes of the LB system. Directly from (5.5), we obtain the fast mode equations

$$\begin{aligned} \frac{\partial R_{11}}{\partial t} + c^2 \frac{\partial (hu)}{\partial x} &= -\lambda (R_{11} - R_{11}^{eq}) \\ \frac{\partial R_{22}}{\partial t} + c^2 \frac{\partial (hv)}{\partial y} &= -\lambda (R_{22} - R_{22}^{eq}). \end{aligned} \tag{5.9}$$

Eqs. (5.6) and (5.9) are analogous to (2.14) and (2.10), respectively. Eq. (4.3, 5.6, 5.9) form a complete set of equations for all 5 modes. Eliminating R_{11} and R_{22} between (5.9) and (5.6), we obtain the analogs of (2.17),

$$\begin{aligned} \lambda[(hu)_t - fhv + ghh_x] + [(hu)_{tt} - f(hv)_t - c^2(hu)_{xx}] &= 0 \\ \lambda[(hv)_t + fhu + ghh_y] + [(hv)_{tt} + f(hu)_t - c^2(hv)_{yy}] &= 0 \end{aligned} \tag{5.10}$$

in which, for simplicity, we have temporarily dropped the wind forcing terms. As in Section 2, the leading order LB dynamics corresponds to λ times the equations of interest plus "textbook" wave equations, now modified by rotation.

For small time step and lattice spacing, the 4-velocity LB dynamics (5.2–3) is equivalent to (4.3) and (5.10). For large enough λ and c, solutions of (5.10) approximately satisfy

$$\begin{aligned}(hu)_t - fhv &= -ghh_x + \nu(hu)_{xx} \\ (hv)_t + fhu &= -ghh_y + \nu(hv)_{yy}\end{aligned} \tag{5.11}$$

where $\nu = c^2/\lambda$. Eqs. (5.11) are analogous to (2.20). The Chapman-Enskog expansion also yields (5.11), but with the more accurate value

$$\nu = \left(\frac{1}{\lambda} - \frac{1}{\lambda_{max}}\right)c^2, \tag{5.12}$$

where $\lambda_{max} = 2/\Delta t$ as before. Eq. (5.12) is analogous to (4.4). The momentum equations (5.11) differ from (4.6) only in the form of the viscosity, which is anisotropic in (5.11). This anisotropy results from the relatively low degree of symmetry of the 4-velocity lattice.

As in the case of (4.6), LB solutions of (5.11) always approach a steady state. In steady state, $\nabla \cdot (h\mathbf{u}) = 0$, and the transport is described by a streamfunction: $h\mathbf{u} = (-\psi_y, \psi_x)$. In the case of (4.6), the streamfunction satisfies

$$\beta\psi_x = curl\left(\frac{h}{h + \delta_E}\tau\right) + \nu\nabla^4\psi \tag{5.13}$$

with boundary conditions of no-normal-flow, and no-slip or no-stress. If h is everywhere much greater than δ_E, then (5.13) reduces to Munk's classic equation, and ψ is determined independently of h; in fact, the 8-velocity PG solution of Figure 3c closely resembles Munk's solution.

In the case of (5.11), the streamfunction satisfies

$$\beta\psi_x = curl\left(\frac{h}{h + \delta_E}\tau\right) + 2\nu\psi_{xxyy}. \tag{5.14}$$

Once again, the viscosity in (5.14) is anisotropic, and accommodates only the single boundary condition of no-normal-flow. (This is obvious from the fact that the general solution of $\psi_{xxyy} = 0$, easily obtained by integrations, contains only 4 arbitrary functions. These 4 functions are completely determined by the requirement that ψ vanish at each of the 4 boundaries.) This property of (5.11) and (5.14), that only boundary conditions of no-normal-flow may be satisfied, is also obvious from the underlying 4-velocity LB dynamics: As shown in Figure 5b, only the particle moving normal to the boundary encounters the boundary. That is, the 4-velocity model lacks the particles striking the boundary at a 45° angle in the 8-velocity model of Figure 2. It is the rebound of these

particles that determines the second boundary condition, no slip or no stress, in the 8-velocity model.

In the case of (5.13), the western boundary layer equation contains only x-derivatives; its thickness is $\delta_M = (\nu/\beta)^{1/3}$. However, in the case of (5.14), the western boundary layer equation is a partial differential equation,

$$\beta\psi_x = 2\nu\psi_{xxyy}. \tag{5.15}$$

From (5.15) we see that the western boundary layer thickness is

$$\delta_s = \frac{2\nu}{\beta l^2}, \tag{5.16}$$

where l is the scale for long-shore variation in ψ, determined by the interior solution. Thus, in the case of the 4-velocity model, the western boundary layer is proportional to the viscosity coefficient, as in Stommel's classic "bottom friction" model.

Figure 6 shows two LB solutions of the PG equations using the 4-velocity model. The geometry and wind forcing are the same as in the 8-velocity solutions of Figures 3 and 4. Figure 6a, depicting a PG solution with mean upper layer thickness equal to 500 m, should be compared with Figures 3c–d. Figure 6b, with mean h equal to 300 m, should be compared to Figure 4c–d. In both 4-velocity solutions, $\lambda = 0.6\,\lambda_{max}$. With $l = L/2\pi$, this corresponds to a western boundary layer thickness (5.16) of 40 km, about 1 lattice spacing. This thickness is about half the western boundary layer thickness of the 8-velocity solutions shown in Figures 3 and 4. At lower viscosities, the 8-velocity models tend to misbehave. Thus the 4-velocity PG solutions of Figure 6 exhibit very thin but stable western boundary layers that take maximum advantage of the limited spatial resolution. However, they also show the effects of the anisotropic friction, particularly at the point in Figure 6b where the separated western boundary current turns northeastward after leaving the coast.

The computational advantage of the 4-velocity PG model is that it requires only half the computation and storage of the 8-velocity model. In three dimensions, the savings would be greater still; the three-dimensional analogue of the 4-velocity model has 6 velocities, whereas the three-dimensional analogue of the 8-velocity model has 26 velocities. To be fair, Frisch *et al.*'s (1986) optimal two-dimensional model, with complete symmetry of the viscosity and Reynolds stress, contains only 6 velocities. However, the face-centered hypercubic lattice—the optimal symmetric lattice for use in 3 dimensions—contains 24 velocities, still 4 times as many as the three-dimensional PG model with anisotropic viscosity. This factor of 4 represents a huge advantage when one considers the daunting challenge of modeling the global ocean in three dimensions. However, there are other, somewhat more philosophical reasons to favor PG over SW.

6. Discussion

In two dimensions, planetary geostrophic dynamics seem somewhat plain and uninteresting in comparison to the richer shallow water dynamics. However, in three dimensions,

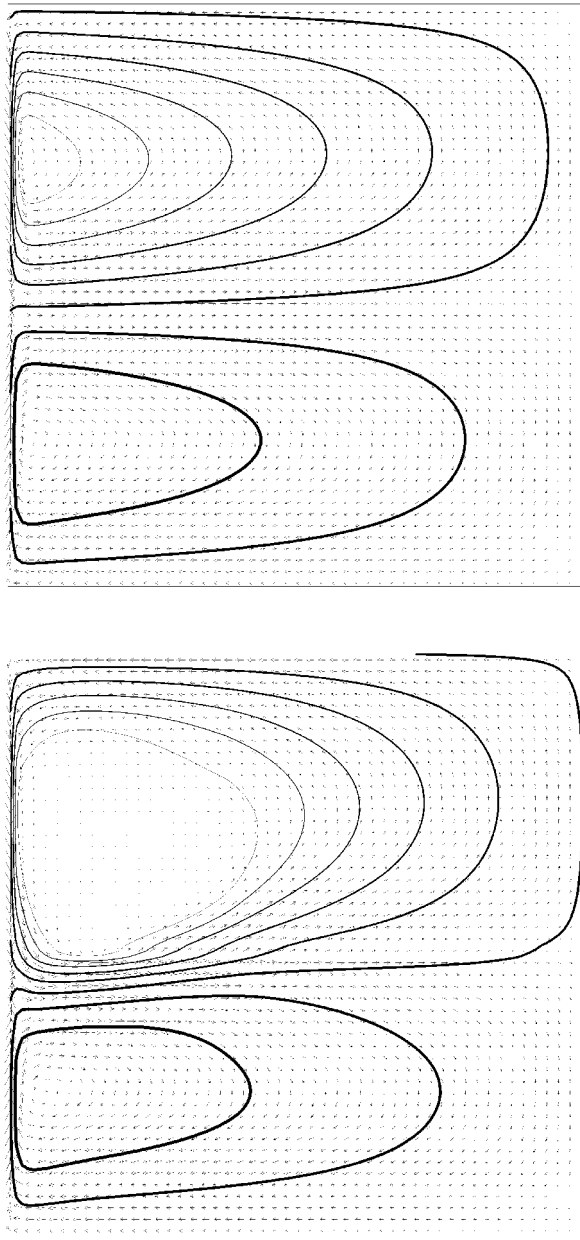

Figure 6. Solutions of the reduced gravity model based upon planetary geostrophic dynamics and the 4-velocity model of Section 5. The forcing and geometry are the same as in the 8-velocity solutions of Figures 3 and 4, but the viscosity now reflects the anisotropy of the underlying lattice. (a) Mean upper layer depth h of 500 m. (b) Mean h of 300 m.

with bathymetry of realistic complexity, solving and understanding planetary geostrophic dynamics will prove to be a considerable challenge. In three dimensions, even *linear* dynamics offer a significant computational challenge; see Salmon (1998b).

The primitive equations (PE)—the three-dimensional analogues of the shallow water equations—may simply be too complex for the present level of dynamical understanding and computational power. In fact, three-dimensional PE admit such a vast range of phenomena that it is conceivable that PE performance may actually degrade as model resolution increases, unless the eddy viscosity is unrealistically large, or the viscous cutoff for molecular viscosity is resolved—an utter impossibility.

For example, consider small-scale Kelvin-Helmholtz instability, an apparently ubiquitous phenomenon in the atmosphere and ocean. If model resolution reaches the point where such instability can occur but is still too coarse to resolve the turbulent cascade that damps the instability, then the instability could become a damaging source of computational noise.[3]

In any case, considering the present state of ignorance about global ocean dynamics, it would seem safest to begin three-dimensional LB modeling with PG dynamics. The three-dimensional analogue of the 4-velocity model in Section 5 offers the advantages of dynamical and computational simplicity, massively parallel construction, and only slightly more dependent variables than in traditional primitive equation models.

Significant difficulties remain. The present method of incorporating the Coriolis force, which makes the LB equations implicit and forces us to use the predictor/corrector method, is accurate but inefficient. I have not yet found an acceptable alternative. A much greater difficulty is that the complex shapes of the real ocean basins seem to require an irregular lattice. Unfortunately, LB methods do not adapt well to irregular lattices. Even the seemingly unavoidable practice of choosing the vertical lattice spacing to be much smaller than the horizontal spacing complicates the LB approach. However, with time and persistence, these difficulties will be overcome. The efficiency and physical simplicity of LB methods are too great to be ignored.

In more conventional numerical modeling, one begins with a relatively simple set of partial differential equations, but the final algorithm is a complicated patchwork of arbitrary steps and compromises that bears only a nebulous relationship to the original differential equations. In the LB method, the algorithm always takes a simple form, and itself acquires the status of an interesting physical system. To investigate its relation to differential equations, we must pursue a relatively complicated analytical expansion, but this is a separate activity, necessary only because of our psychological need to associate models with differential equations.

Acknowledgments. This work was supported by the National Science Foundation, grant OCE-9521004. It is a pleasure to thank Glenn Ierley and George Veronis for helpful comments, and Breck Betts for his help with the figures.

3. Similar ideas were expressed to me by M. J. P. Cullen.

APPENDIX

Motivated derivation of (3.13–15)

In lattice gas theory, the local equilibrium state (3.10) is defined to be that set $\{h_i(\mathbf{x})\}$ that maximizes an entropy, subject to the constraints (3.7) and (3.8) corresponding to mass and momentum conservation. The entropy takes the form that occurs in the H-theorem for the lattice gas. However, if, as here, we begin at the level of the Boltzmann equation, with no precisely defined lattice gas in mind, then the form of the entropy is somewhat arbitrary. In this circumstance, it is perhaps logical to define h^{eq} as that set of populations which maximizes the information-theoretic entropy

$$\sum_i h_i(\mathbf{x}) \ln h_i(\mathbf{x}) \tag{A1}$$

at lattice point $\mathbf{x}$, subject to (3.7) and (3.8). The resulting equilibrium state is a well-determined function of $h(\mathbf{x})$, $u(\mathbf{x})$, and $v(\mathbf{x})$ at each lattice point. However, the exact solution to this variational problem is quite difficult, and one normally proceeds by means of an expansion in which u and v are presumed to be small. From symmetry considerations, this expansion takes the form

$$h_i^{eq}(h, u, v) = A(h) + B(h)c_{i\alpha}u_\alpha + C(h)c_{i\alpha}c_{i\beta}u_\alpha u_\beta + D(h)\delta_{\alpha\beta}u_\alpha u_\beta + \mathrm{O}(\mathbf{u}^3). \tag{A2}$$

The coefficients A, B, C and D depend only on h—not $\mathbf{u}$—and are uniquely determined by the maximum entropy principle. However, 3 of these 4 coefficients would be determined by the constraints (3.7–8) alone, and the truncation of (A2) at quadratic order has somewhat the same effect as demanding that the entropy be maximum. Thus it makes sense to demand only that (A2) satisfy (3.7–8) for arbitrary h and (small) $\mathbf{u}$. This leaves one of the coefficients in (A2) undetermined, but the freedom to adjust this parameter is very helpful at a later stage.

In fact, as previous workers have found, it proves very handy to generalize (A2) even further, by demanding that (A2) hold with coefficients $A(h)$, $B(h)$, $C(h)$, and $D(h)$ that are different for the three different classes of particle—the rest particle, the 4 particles moving in the coordinate directions, and the 4 particles moving diagonally. Thus we assume

$$h_0^{eq}(h, u, v) = A_0(h) + D_0(h)\delta_{\alpha\beta}u_\alpha u_\beta \tag{A3}$$

for the equilibrium rest-particle population,

$$h_i^{eq}(h, u, v) = A(h) + B(h)c_{i\alpha}u_\alpha + C(h)c_{i\alpha}c_{i\beta}u_\alpha u_\beta + D(h)\delta_{\alpha\beta}u_\alpha u_\beta, \qquad i \text{ odd} \tag{A4}$$

for the particles moving in the 4 coordinate directions, and

$$h_i^{eq}(h, u, v) = \overline{A}(h) + \overline{B}(h)c_{i\alpha}u_\alpha + \overline{C}(h)c_{i\alpha}c_{i\beta}u_\alpha u_\beta + \overline{D}(h)\delta_{\alpha\beta}u_\alpha u_\beta, \qquad i \text{ even} \tag{A5}$$

for the particles moving in the 4 diagonal directions. Altogether there are 10 coefficients to be determined. Substituting (A3–A5) into (3.16) and equating the coefficients of h and

$\mathbf{u} \cdot \mathbf{u}$, we obtain

$$A_0 + 4A + 4\overline{A} = h \tag{A6}$$

and

$$D_0 + 2c^2C + 4c^2\overline{C} + 4D + 4\overline{D} = 0. \tag{A7}$$

Similarly, (3.17) implies

$$2c^2B + 4c^2\overline{B} = h. \tag{A8}$$

From (3.18) we obtain the 4 conditions

$$2c^4C = 8c^4\overline{C} = h \tag{A9}$$

$$2c^2A + 4c^2\overline{A} = \tfrac{1}{2}gh^2 \tag{A10}$$

$$2c^2D + 4c^2\overline{D} + 4c^4\overline{C} = 0. \tag{A11}$$

Finally, the identity

$$\frac{\partial}{\partial x_\gamma}\sum_i c_{i\alpha}c_{i\beta}c_{i\gamma}h_i^{eq} = \frac{1}{3}c^2\left\{\nabla\cdot(h\mathbf{u})\delta_{\alpha\beta} + \frac{\partial}{\partial x_\alpha}(hu_\beta) + \frac{\partial}{\partial x_\beta}(hu_\alpha)\right\} \tag{A12}$$

needed to reduce the viscous tensor (3.34) to the form (3.35) requires that

$$B = 4\overline{B}. \tag{A13}$$

In deriving these equations, it is useful to realize that

$$\sum_i c_{i\alpha} = \sum_i c_{i\alpha}c_{i\beta}c_{i\gamma} = \cdots = 0, \tag{A14}$$

$$\sum_i c_{i\alpha}c_{i\beta} = 6c^2\delta_{\alpha\beta}, \tag{A15}$$

and

$$\sum_i c_{i\alpha}c_{i\beta}c_{i\gamma}c_{i\delta} = 4c^4(\delta_{\alpha\beta}\delta_{\gamma\delta} + \delta_{\alpha\gamma}\delta_{\beta\delta} + \delta_{\alpha\delta}\delta_{\beta\gamma}) - 6c^4\delta_{\alpha\beta\gamma\delta}. \tag{A16}$$

The peculiar form of (A16) results from the anisotropy of the rectangular lattice.

We now have 8 equations for the 10 undetermined coefficients. Thus we are free to impose 2 additional conditions. Eqs. (A9) and (A13) suggest the additional conditions,

$$A = 4\overline{A} \quad \text{and} \quad D = 4\overline{D}. \tag{A17}$$

These make all the coefficients in (A5) one fourth the size of the corresponding coefficients in (A4). Then, solving for all the coefficients, we obtain (3.13–15). Note that, for sufficiently small positive h, half of the populations (3.14–15) actually become *negative.*

REFERENCES

Ancona, M. G. 1994. Fully-Lagrangian and Lattice-Boltzmann methods for solving systems of conservation equations. J. Comp. Phys., *115,* 107–120.

Benzi, R., S. Succi and M. Vergassola. 1992. The lattice Boltzmann-equation—theory and applications. Phys. Rep., *222,* 145–197.

Benzi, R., F. Toschi and R. Tripiccione. 1998. On the heat transfer in Rayleigh-Benard systems. J. Stat. Phys., *93,* 901–918.

Chen, S. and G. D. Doolen. 1998. Lattice Boltzmann method for fluid flows. Ann. Rev. Fluid Mech., *30,* 329–364.

Frisch, U., B. Hasslacher and Y. Pomeau. 1986. Lattice-gas automata for the Navier-Stokes equations. Phys. Rev. Lett., *56,* 1505–1508.

Parsons, A. T. 1969. A two-layer model of Gulf Stream separation. J. Fluid Mech., *39,* 511–528.

Rothman, D. H. and S. Zaleski. 1997. Lattice-Gas Cellular Automata: Simple Models of Complex Hydrodynamics, Cambridge, 297 pp.

Salmon, R. 1998a. Lectures on Geophysical Fluid Dynamics, Oxford, 378 pp.

—— 1998b. Linear ocean circulation theory with realistic bathymetry. J. Mar. Res., *56,* 833–884.

Veronis, G. 1973. Model of world ocean circulation: I. Wind-driven, two-layer. J. Mar. Res., *31,* 228–288.

—— 1980. Dynamics of large-scale ocean circulation, *in* Evolution of Physical Oceanography, B. A. Warren and C. Wunsch, eds., 140–183.

Received: *6 October, 1998;* revised: *9 February, 1999.*